A FAST VISCOUS CORRECTION METHOD FOR FULL-POTENTIAL TRANSONIC WING ANALYSIS

ICAS-84-1.2.3

Shen C. Lee
University of Missouri, Rolla, Missouri
Scott D. Thomas
Informatics General Corporation, Palo Alto. California
and
Terry L. Holst
NASA Ames Research Center, Moffett Field, California

ABSTRACT

A viscous correction method was developed for the three-dimensional full-potential transonic wing analysis code, TWING. The viscous effect in the near wake region downstream of the trailing edge was considered in TWING by imposing the Kutta condition that the rear stagnation point is at the trailing edge for the lifting as well as for the non-lifting cases. TWING used a fast iteration scheme which gave good results for swept, tapered and twisted wings as long as the shock is relatively weak. The objective of this study is to improve the accuracy for moderately-strong shock situations without substantially increasing the computational time. The shock/boundary-layer interaction along the wing surface was considered by superpositioning a viscous ramp at the foot of the shock on a boundary-layer displacement thickness obtained from a conventional integral boundary-layer method. The effective displacement thickness was then related to a vertical component of the surface velocity which was implemented as a transpirational boundary condition. Viscous solutions were obtained and compared with inviscid solutions as well as with experimental data. For weak shock situations, the viscous correction is not necessary because it took approximately 10% additional computer time and gave no significant improvement from the inviscid solution. For moderately-strong shock situations, the viscous correction improved the accuracy on shock position and pressure distribution with 13% and 3% additional computer time for the ONERA M6 wing and the Wing A, respectively.

I. INTRODUCTION

The cost for development of transonic aircrafts has been greatly reduced by the extensive use of numerical simulation. Currently, there are two different approaches in numerical analysis of transonic flows: The viscous approach and the inviscid approach. The viscous approach is physically more appropriate; but numerically it takes too much computational time for practical applications. For example, Pulliam and Steger (1) solved the thin layer equations for transonic flow about axially symmetric bodies; Steger (2) solved the Reynolds equations for transonic flow about airfoils. The required computer time makes it unpractical to use these methods for analyzing three-dimensional wings with the current generation of computers. The inviscid approach, on the other hand, is physically neglecting the effect of friction; but numerically it is very efficient in transonic flow simulations when the shock wave is relatively weak. For example, Ballhaus and Goorjian (3) solved the unsteady small-disturbance equation for airfoils maneuvering at low frequency unsteady motions; Holst (4) solved the full-potential equation for airfoils at steady flight. The required computational time was about two orders of magnitude less than that of the viscous approach. However, for moderately-strong shock situations, inviscid approach encountered dificulties in determining the actual shock locations.

Several viscous/inviscid interaction methods have been developed to correct this problem. Yoshihara and Zonars (5) used a viscous ramp to simulate the suddenly thickened boundary layer behind the shock. It resulted in a more realistic shock position with practically no increase in computational time, because the viscous-ramp contour was obtained from a simple empirical relation. However, the ramp, which was inserted at the foot of the shock, needed to have a "precurser" for smooth transition in order to provide numerical stability. Moreover, the ramp neglected the viscous effect before the shock. Boundary-layer calculations for an aerodynamic body at transonic flight was conducted by many investigators. Nash and Scruggs (6) solved the differential boundary layer equations for three-dimensional wings. It gave good results for the boundary-layer development before the shock; but it failed to make any significant improvement for the shock location, because it was necessary to modify the adverse pressure gradient after the shock in order to keep the boundary-layer assumptions valid. Moreover, the computational time was too long so that the computational efficiency of the inviscid approach became irrelevant. Melnik et. al (7) used the lag-entrainment method which was developed by Green et. al (8) by solving the integral boundary-layer equations together with an "integral" turbulent kinetic energy equation. It allowed the shape factor to go above the limit of separation beyond which the boundary-layer assumptions are not valid. Nevertheless, the boundary layer behind the shock could grow thicker and the location of the shock was improved from the inviscid solution. However, the amount of computational time required was more than three times of the inviscid solution. Moreover, the lag-entrainment method required a large number of empirical constants which were not able to be experimentally varified. A conventional integral boundary-layer method was developed by Sasman and Cresi (9) for both subsonic and supersonic flows. It used a Mager (10) transformation to consider the density variations due to the temperature gradient in the boundary layer and solved the momentum and the moment-of-momentum equations with a fourth order Runge-Kutta method. The wall shear stress model was verified by Tetervin (11). This method was coded by McNally (12) as BLAYER to include a laminar boundary layer at the leading edge. BLAYER, which required less computational time than both the differential boundary layer method and the integral lag-entrainment method, gave good

results before the shock. However, BLAYER, which modified the adverse pressure gradient behind the shock to avoid flow separation, became inadequate to locate the shock position.

In order to consider the suddenly thickened boundary layer behind the shock and the conventional boundary-layer before the shock, Lee and Van Dalsem (13) used an empirical relation to combine the contours of the viscous ramp (5) and the boundary-layer displacement thickness (12) to develop a viscous correction method for a two-dimensional, steady, full-potential solution (4). Lee (14) used the same concept for a viscous correction method of a two-dimensional, unsteady, small-disturbance solution (3). The results of these viscous correction methods not only improved the accuracy of the inviscid solutions but also reduced the computational time by reducing the number of supersonic points in the flowfield during the iteration process. This study is to apply the same concept to the three-dimensional transonic wing analysis using a strip method which considers the boundary-layer growth along the streamwise direction but neglects that of the spanwise direction.

II. TRANSONIC WING ANALYSIS

A transonic wing analysis was conducted by Holst and Thomas (15). The code TWING was developed using an implicit approximate factorization algorithm to solve the three-dimensional full-potential equation. Comparing with the inviscid code FL028 developed by Caughey and Jameson (16), TWING gave identical results with one-tenth of the computational time. Since the viscous effect of shock/boundary-layer interaction was neglected, it was expected that the numerical results would deviate from experimental data for moderately-strong shock situations. Consequently, a viscous correction method is needed not only to improve the accuracy of the inviscid solution but also to maintain its computational efficiency.

The three-dimensional full-potential equation written in strong conservation-law form is given as:

$$(\rho\Phi_x)_x + (\rho\Phi_y)_y + (\rho\Phi_z)_z = 0 \tag{1}$$

where ρ is the non-dimensionalized density which can be written as:

$$\rho = [1 - \frac{\gamma - 1}{\gamma + 1}(\Phi_x^2 + \Phi_y^2 + \Phi_z^2)]^{\frac{1}{\gamma - 1}} \tag{2}$$

In these equations, the non-dimensionalized velocity components Φ_x, Φ_y and Φ_z are expressed in terms of the first derivatives of the velocity potential in their respective directions; x, y and z are the Cartesian coordinates in the streamwise, spanwise and vertical directions, respectively; and γ is the specific heat ratio. The characteristic quantities for non-dimensionalization are the stagnation density, ρ_o, the critical speed of sound, a*, and the chord length, c.

Equations (1) and (2) are transformed from the physical domain, x, y, and z, to the computational domain, ξ, η, and ζ, by using a general independent-variable transformation, they become:

$$(\rho U/J)_\xi + (\rho V/J)_\eta + (\rho W/J)_\zeta = 0 \tag{3}$$

$$\rho = [1 - \frac{\gamma - 1}{\gamma + 1}(U\Phi_\xi + V\Phi_\eta + W\Phi_\zeta)]^{\frac{1}{\gamma - 1}} \tag{4}$$

where the contravariant velocities are:

$$\begin{aligned} U &= A_1\Phi_\xi + A_4\Phi_\eta + A_5\Phi_\zeta \\ V &= A_4\Phi_\xi + A_2\Phi_\eta + A_6\Phi_\zeta \\ W &= A_5\Phi_\xi + A_6\Phi_\eta + A_3\Phi_\zeta \end{aligned} \tag{5}$$

the coefficient matrix of the contravariant velocity may be written as:

$$\begin{aligned} A_1 &= \nabla\xi^2 & A_2 &= \nabla\eta^2 \\ A_3 &= \nabla\zeta^2 & A_4 &= \nabla\xi\cdot\nabla\eta \\ A_5 &= \nabla\xi\cdot\nabla\zeta & A_6 &= \nabla\eta\cdot\nabla\zeta \end{aligned} \tag{6}$$

The transformation between the physical domain and the computational domain is shown schematically in Figure 1. The wing surface is the plane of $\zeta = \zeta_{max}$. The upper and lower vortex sheets in the wake region are $\zeta = \zeta_{min}$ and $\zeta = \zeta_{max}$, respectively. The spanwise cross-sections are the planes of η = constant which coincide with the planes of y = constnat, or

$$y_\xi = 0, \qquad y_\zeta = 0 \tag{7}$$

The spanwise cross-section next to the fuselage can be considered as the plane of symmetry, $\eta = \eta_{min}$. The spanwise cross-section beyond the wing tip, $\eta > \eta_{tip}$, is assumed to be an extension of the wing with zero thickness. The Jacobian of transformation can be written as:

$$J = (\xi_x\zeta_z - \xi_z\zeta_x)\eta_y = 1/(x_\xi z_\zeta - z_\xi x_\zeta)y_\eta \tag{8}$$

A body-fitted grid may then be generated, at each spanwise cross-section, from the solution of the following two Lapace equations:

$$\begin{aligned} \xi_{xx} + \xi_{zz} &= 0 \\ \zeta_{xx} + \zeta_{zz} &= 0 \end{aligned} \tag{9}$$

A grid of 89 x 25 x 18 is used in this study. A typical three-dimensional grid is shown in Figure 2. It is noted that an O-grid in the ξ-direction is used for maximum effectiveness at a minimum number of grid points. Detailed discussions on the grid generation, the spatial differencing, the alternating directional implicit procedure and the approximate factorization scheme were given by Holst and Thomas (15). The solution is obtained when the residual of Equation (3) is within an accpetable tolerance. To consider the viscous effect, this study uses the same general approach with a modified boundary condition along the wing surface as well as along the vortex sheets downstream of the trailing edge.

III. VISCOUS EFFECT

The three-dimensionality of the wing, due to swept-back, tapering and twist, was considered by the inviscid solution which provided the boundary

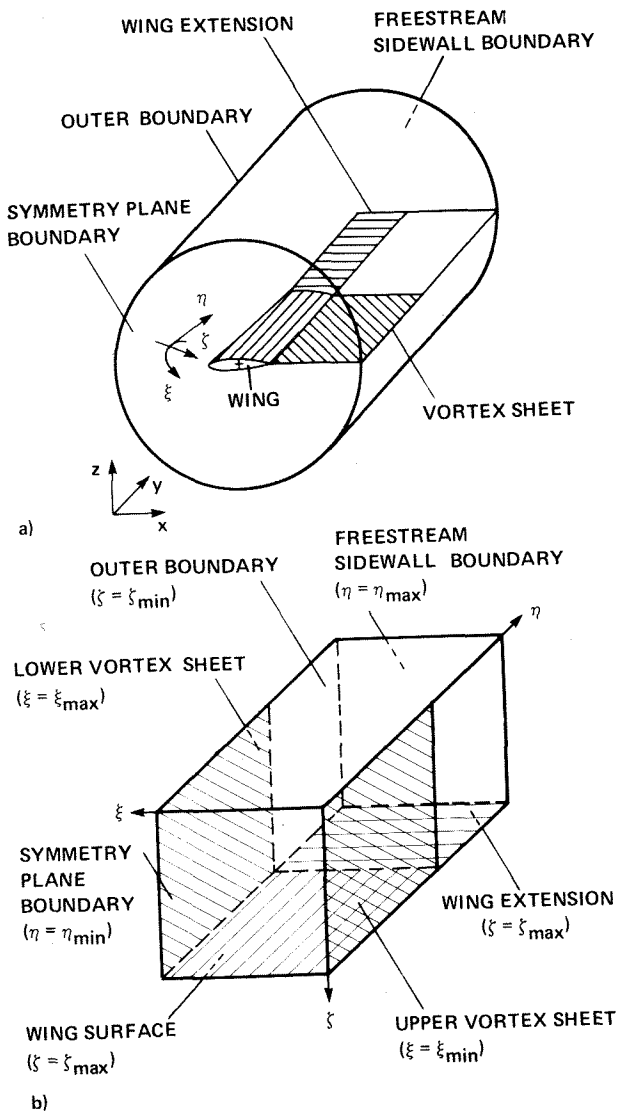

Figure 1. Coordinate Transformation
a) Physical Domain (x,y,z)
b) Computational Domain (ξ,η,ζ)

condition at the freestream for the boundary-layer solution. Using a strip method which considers only the viscous effect along the streamwise direction, a two-dimensional boundary layer was calculated at each cross-section of the wing span. The same principle used by Lee and Van Dalsem (13) for viscous correction about airfoils may then be used for three-dimensional wings by superpositioning a viscous ramp at the foot of the shock on a turbulent boundary layer.

A. Boundary Layer

Near the leading edge, there is a laminar boundary-layer region, which is followed by a transition region and a turbulent region. In transonic flow, the laminar and transition regions are very small, and their effect on aerodynamic performances are insignificant. A simple approach proposed by Cohen and Roshotko (17) was used to provide the initial condition for the turbulent boundary layer. Assuming that transition occurs instantaneously at a very short distance downstream of the leading edge, the integral method of Sasman and Cresi (9) was used for computing the turbulent boundary layer. The time-averaged continuity and momentum euquations for a two-dimensional, steady, compressible, turbulent boundary layer can be expressed as:

$$(\rho u)_s + (\rho w)_n = 0 \tag{10}$$

$$\rho u(u)_s + \rho w(u)_n = -(p)_s + (\tau)_n \tag{11}$$

In these equations, u and w are the time-averaged velocity components in the streamwise, s, and its normal, n, directions, respectively, and τ is the shear stress. Using the Mager transformation (10) to consider the temperature variation for transonic flow in the boundary layer, the transformed coordinates are:

$$\hat{s} = \int_0^s \left(\frac{T_o}{\bar{T}}\right)\left(\frac{T_e}{T_o}\right)^{(\gamma+1)/[2(\gamma-1)]} \tag{12}$$

$$\hat{n} = \left(\frac{T_e}{\bar{T}_o}\right)^{\frac{1}{2}} \int_0^n \frac{\rho}{\rho_o}\, dn \tag{13}$$

where the subscripts e and o denote the edge of the boundary layer and the stagnation condition, respectively. The reference temperature $\bar{T}$ is given as a function of the Prandtl number, Pr,

$$\frac{\bar{T}}{T_o} = 0.5\,\frac{T_w}{T_o} + 0.22\,Pr^{\frac{1}{3}} + (0.5 - 0.22\,Pr^{\frac{1}{3}})\left(\frac{T_e}{T_o}\right)$$

where the subscript w denotes the wall condition. The shape factor, H, and the momentum thickness, θ, are related to the transformed shape factor, $\hat{H}$, and the transformed momentum thickness, $\hat{\theta}$, as:

$$H = \frac{T_w}{T_o}\left[1 - \frac{\gamma-1}{2}M_e^2\right]\hat{H} + \frac{\gamma-1}{2}M_e^2 \tag{15}$$

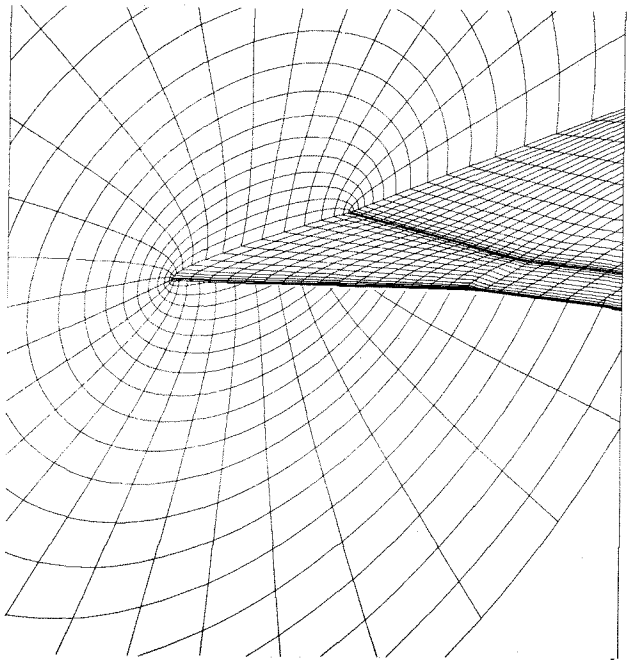

Figure 2. Perspective View of the Wing Grid

$$\theta = \left[\frac{T_o}{T_e}\right]^{(\gamma+1)/[2(\gamma-1)]} \hat{\theta} \tag{16}$$

$$\text{with} \qquad H = \frac{\delta^*}{\theta} \tag{17}$$

where M is the Mach number. The boundary-layer displacement thickness, δ^*, is related to the transformed displacement thickness, $\hat{\delta}^*$, by the relation of:

$$\delta^* = (\hat{\theta} + \hat{\delta}^*)\left(\frac{T_o}{T_e}\right)^{(3\gamma-1)/[2(\gamma-1)]} - \hat{\theta}\left(\frac{T_o}{T_e}\right)^{(\gamma+1)/[2(\gamma-1)]} \tag{18}$$

For an adiabatic flow, the transformed displacement thickness and momentum thickness becomes:

$$\hat{\delta}^* = \int_o^{\hat{\delta}} \left(1 - \frac{\hat{U}}{U}\right) d\hat{n} \tag{19}$$

$$\hat{\theta} = \int_o^{\hat{\delta}} \frac{\hat{U}}{U_e}\left(1 - \frac{\hat{U}}{U_e}\right) d\hat{n} \tag{20}$$

where $\hat{\delta}$ is the boundary layer thickness in the transformed coordinates, and U is the transformed velocity component in the $\hat{s}$ direction with

$$\hat{U} = u\left(\frac{T_o}{T_e}\right)^{\frac{1}{2}} \tag{21}$$

The transformed velocity profile in the boundary layer also obeys the power law:

$$\frac{\hat{U}}{U_e} = \left(\frac{\hat{n}}{\hat{\delta}}\right)^{(\hat{H}_i - 1)/2} \tag{22}$$

where the adiabatic shape factor, $\hat{H}_i$, is defined as:

$$\hat{H}_i = \frac{\hat{\delta}^*}{\hat{\theta}} \tag{23}$$

The transformed momentum integral equation can be written as:

$$\frac{d\hat{\theta}}{ds} + \frac{\hat{\theta}}{U_e}\frac{dU_e}{ds}\left(2 + \frac{T_w}{T_o}\hat{H}_i\right) = \left(\frac{T_o}{T_e}\right)^{0.268}\left(\frac{T}{T_o}\right)^{1.268}\frac{\tau_w}{\rho_e U_e^2} \tag{24}$$

The transformed moment-of-momentum equation then becomes:

$$\frac{d\hat{H}_i}{ds} = -\frac{1}{2U_e}\frac{dU_e}{ds}(\hat{H}_i + 1)^2(\hat{H}_i - 1)\left[1 + \left(\frac{\tau_w}{T_o} - 1\right)\frac{H_i^2 + 4H_i - 1}{(H_i+1)(H_i+3)}\right] + \frac{H_i^2 - 1}{\theta}\left(\frac{T}{T_e}\right)\left[\frac{H_i \tau_w}{\rho_e U_e^2} - (H_i + 1)\int_o^1 \frac{\tau}{\tau_w}\, d\left(\frac{\hat{n}}{\delta}\right)\right] \tag{25}$$

The shear stress at the wall, τ_w, is expressed through an empirical relation given by Tetervin (11) as:

$$\tau_w = 0.123\,\rho_e U_e^2 \left(\frac{U_e \theta}{\nu}\right)^{-0.268}\left(\frac{T_e}{T}\right)^{1.268} e^{-1.561 H_i}$$

where ν is the kinematic viscosity at temperature T. The two ordinary differential equations, equations (24) and (25), can be solved simultaneously using the fourth order Runge-Kutta method. The boundary layer displacement thickness, δ^*, can then be obtained from equation (18). This method gives good results as long as there is no flow separation. However, when shock wave and boundary layer interact, strong adverse pressure gradient occurs. In order to locate the shock position adequately with a minimum amount of computational time, the concept of viscous ramp (5) was adopted for the region behind the shock.

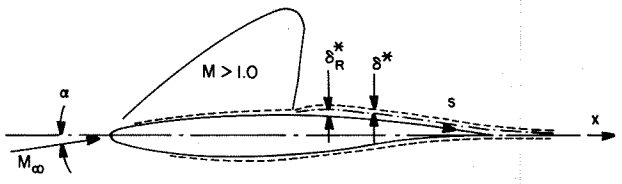

Figure 3. Viscous/Inviscid Interaction at a given spanwise Cross-section

B. Viscous Ramp

An empirical formula, which simulates the suddenly thickened boundary layer behind the shock, was developed by Lee and Van Dalsem (13) for transonic flow about airfoils. The same concept can be used for transonic wings at each spanwise cross-section. The thickness of the ramp, δ^*_R, is expressed as a function of s:

$$\frac{\delta^*_R(s)}{c} = \begin{cases} 0, & \text{for } s < s_{sh} \\ \beta_1 \theta_{max}\left\{1 - \exp[s_{sh} - s]/c\beta_1\right\}, & s \geq s_{sh} \end{cases} \tag{27}$$

where β_1 is a constant. ($\beta_1 = 0.1$ has been used for all cases.) The term θ_{max} represents the maximum deflection angle for an attached shock at a given upstream Mach number which is determined by the inviscid solution. The subscript sh denotes the location of the shock in the streamwise direction at each spanwise cross-section. Figure 3 shows the method of superposition at each spanwise cross-section. The effective displacement thickness, δ^*_{eff}, was obtained by the relation:

$$\delta^*_{eff} = \begin{cases} \delta^*, & \text{for } s < s_{sh} \\ (\delta^* + \delta^*_R)/2, & \text{for } s \geq s_{sh} \end{cases} \tag{28}$$

Using the suggestion of Lighthill (18), a vertical component of the surface velocity, w_v, can be obtained from the effective displacement thickness as follows:

$$w_v = (\rho u \delta^*_{eff})_s / \rho \tag{29}$$

where the subscript s denotes the first derivative in the streamwise direction along the surface. It is noted that the computational time for δ^* is much larger than that for δ^*_R, while the variation for δ^* is insignificant during each successive iteration as long as the residual of Equation (3) is within an order of magnitude of the acceptable tolerance. In order to minimize the computational time without sacrificing the computational accuracy, δ^*_R was calculated at every iteration while δ^* was calculated only once when the residual of Equation (3) is less than or equal to ten times of the acceptable value at each spanwise cross-section. Detailed discussions on computational time versus computational accuracy was given by Lee (14) for viscous corrections of unsteady transonic airfoil analysis.

To begin the iteration process, the flow is assumed to be inviscid. TWING calculates the contravariant velocity and the density distributions of the flowfield. Using these values as the boundary condition for the viscous effect, the effective displacement thickness, δ^*_{eff}, can be obtained. The values of the vertical component of the surface velocity, w_v, may then be calculated and implemented as the boundary condition for the next iteration.

IV. BOUNDARY CONDITION

Along the wing surface, $\zeta = \zeta_{max}$, as well as along the vortex sheets, $\xi = \xi_{min}$ and $\xi = \xi_{max}$, the viscous effect can be analyzed as follows:

A. Along the Wing Surface

The gradient of the velocity potential at $\zeta = \zeta_{max}$ can be expressed as:

$$\nabla\Phi_{ws} = w_v \tag{30}$$

where the subscript ws denotes the wing surface. Since the contravariant velocity component in the ζ-direction can also be written as:

$$W = \nabla\zeta \cdot \nabla\Phi \tag{31}$$

with w_v and ζ in the opposite direction at $\zeta = \zeta_{max}$, the boundary condition along the wing surface then becomes:

$$W_{ws} = -\sqrt{A_3}\, w_v \tag{32}$$

To evaluate the boundary condition for the contravariant velocity components in the ξ and η directions, it is necessary to separate the spanwise cross-section of symmetry, $\eta = \eta_{min}$, from the other spanwise cross-sections, $\eta_{min} < \eta < \eta_{tip}$.

1. $\eta = \eta_{min}$

The cross-section next to the fuselage, or the cross-section of symmetry, has no velocity component in the η-direction:

$$V_{ws} = 0 \tag{33}$$

Substituting equations (32) and (33) into equation (5), the components of Φ_η and Φ_ζ can be related to Φ_ξ and w_v along the surface as:

$$\Phi_\eta = \frac{(A_5A_6 - A_3A_4)\,\Phi_\xi + A_6\sqrt{A_3}\, w_v}{A_2A_3 - A_6A_6} \tag{34}$$

$$\Phi_\zeta = \frac{(A_4A_6 - A_2A_5)\,\Phi_\xi - A_2\sqrt{A_3}\, w_v}{A_2A_3 - A_6A_6} \tag{35}$$

The contravariant velocity component in the ξ-direction becomes:

$$U_{ws} = \left(A_1 + \frac{2A_4A_5A_6 - A_3A_4A_4 - A_2A_5A_5}{A_2A_3 - A_6A_6}\right)\Phi_\xi + \frac{A_4A_6\sqrt{A_3} - A_2A_5\sqrt{A_3}}{A_2A_3 - A_6A_6}\, w_v \tag{36}$$

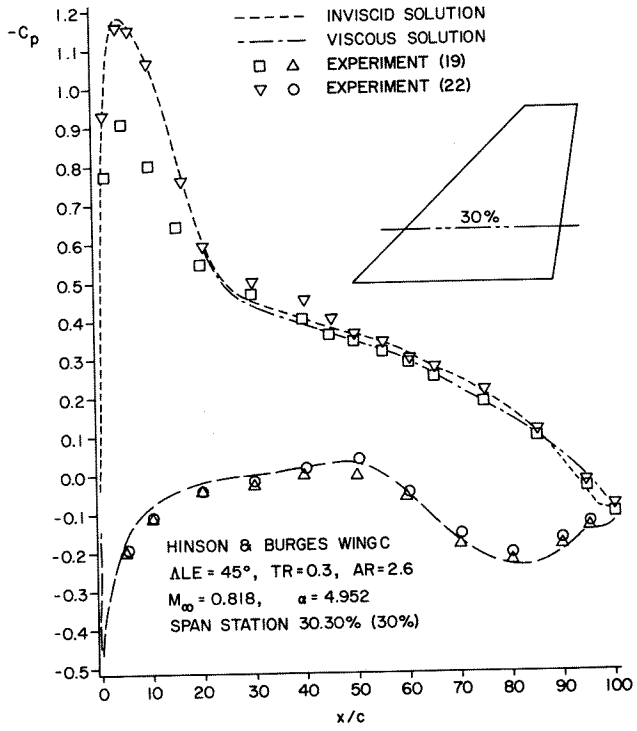

Figure 4. Pressure Coefficient, Wing C, η = 30%

2. $\eta > \eta_{min}$

At any other spanwise cross-section along the surface, only equation (32) is valid. The component of Φ_ζ will have to be expressed as a function of Φ_ξ, Φ_η and w_v as follows:

$$\Phi_\zeta = -\frac{A_5\Phi_\xi + A_6\Phi_\eta + \sqrt{A_3}\, w_v}{A_3} \tag{37}$$

The boundary conditions for the contravariant velocity components in the ξ and η directions become:

$$U_{ws} = (A_1 - \frac{A_5A_5}{A_3})\Phi_\xi + (A_4 - \frac{A_5A_6}{A_3})\Phi_\eta - \frac{A_5}{\sqrt{A_3}}w_v \quad (38)$$

$$V_{ws} = (A_4 - \frac{A_6A_5}{A_3})\Phi_\xi + (A_2 - \frac{A_6A_6}{A_3})\Phi_\eta - \frac{A_6}{\sqrt{A_3}}w_v \quad (39)$$

It is noted that the boundary conditions of all the contravariant velocity components are identical to those of the inviscid flow, if the normal component of the surface velocity, w_v, is zero. In other words, the boundary layer may be considered as a contributor of a small-disturbance velocity-potential. Equation (37) may also be written as:

$$\Phi_\zeta = \bar{\Phi}_\zeta + \phi'_\zeta \quad (37a)$$

where $\bar{\Phi}_\zeta$ is the inviscid velocity-potnetial and ϕ'_ζ is the small-disturbance velocity-potential with

$$\phi'_\zeta = -\frac{w_v}{\sqrt{A_3}} \quad (37b)$$

Consequently the small-disturbance contravariant velocity components along the wing surface become:

$$U'_{ws} = -\frac{A_5}{\sqrt{A_3}}w_v \quad (38b)$$

$$V'_{ws} = -\frac{A_6}{\sqrt{A_3}}w_v \quad (39b)$$

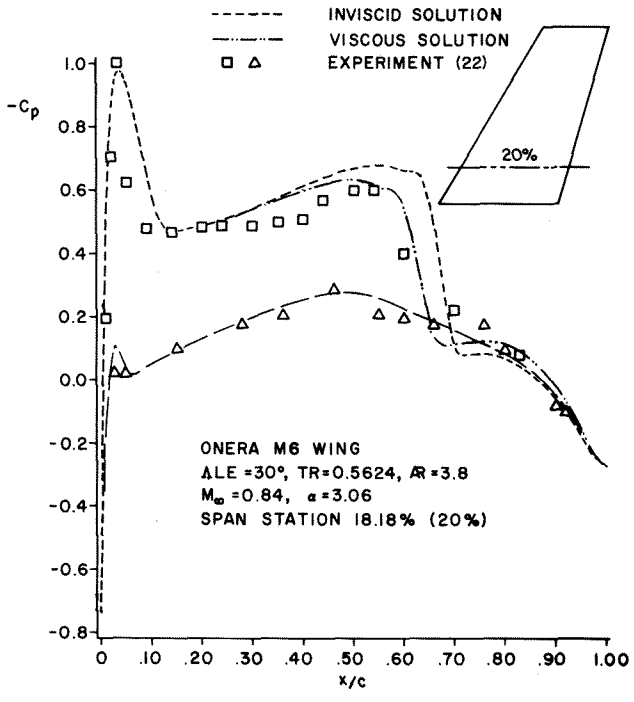

Figure 5. Pressure Coeficient, Wing M6, η = 30%

$$W'_{ws} = -\sqrt{A_3}\,w_v \quad (32b)$$

The same concept can also be applied along the vortex sheets in the wake region.

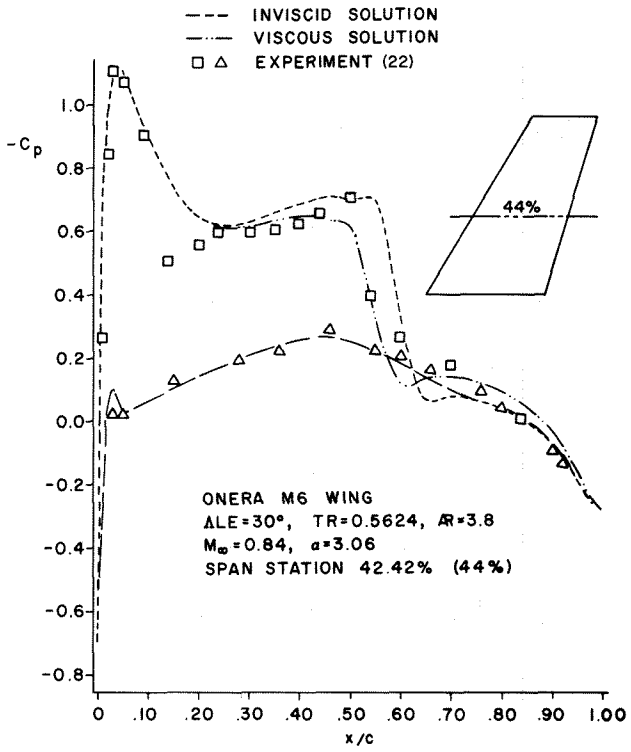

Figure 6. Pressure Coeficient, Wing M6, η = 44%

B. In the Wake Region

Considering the vortex sheets downstream of the trailing edge as an extension of the wing surface, TWING assumed that the Kutta condition was satisfied at the trailing edge. Introducing the strength of circulation at each spanwise cross- section, Γ_j, the rear stagnation point was held at the trailing edge for the lifting case as well as for the non-lifting case. Detailed discussion of the circulation algorithum was given by Holst and Thomas (15). The physical significance is that the viscous effect of the lifting case in the wake region is included in the inviscid solution of TWING. Consequently, the effect of the boundary layer for the lifting case can be considered the same way as that for the non-lifting case.

For the non-lifting case, the effective boundary layer thickness, δ^*_{eff}, along the vortex sheet can also be assumed as an extension of the surface boundary-layer thickness which diminishes rapidly as it enters into the wake region. The structure of the O-grid requires the upper and the lower vortex sheets be analyzed separately. The surface velocity normal to the the upper vortex sheet, w_v, is in the same direction as the contravariant velocity in the ξ-direction. Using the same idea for equation (37b), the small-disturbance velocity-potential along the upper vortex sheet, $(\phi'_\xi)_{uvs}$, can be written as:

$$(\phi_{\xi}')_{UVS} = \frac{w_v}{\sqrt{A_1}} \tag{40}$$

The surface velocity normal to the lower vortex sheet, w_v, is in the opposite direction as the contravariant velocity in the ξ-direction, or

$$(\phi_{\xi}')_{LVS} = -\frac{w_v}{\sqrt{A_1}} \tag{41}$$

Using the analogies of equations (38b), (39b), and (32b), the small-disturbance contravariant velocity components along the vortex sheets become:

$$U_{vs}' = \pm \sqrt{A_1}\, w_v \tag{42}$$

$$V_{vs}' = \pm \frac{A_4}{\sqrt{A_1}} w_v \tag{43}$$

$$W_{vs}' = \pm \frac{A_5}{\sqrt{A_1}} w_v \tag{44}$$

where the subscript vs designates vortex sheets with the positive sign for the upper and the negative sign for the lower vortex sheets, respectively. It is noted that the imposed Kutta condition at the trailing edge considers the viscous effect of the lifting case. Consequently, the values of w_v in the wake has no significant influence to the pressure coefficient on the wing surface. In order to provide a smooth transition from the wing surface to the vortex sheets, the value of w_v was assumed to decrease by 25% at each grid point from the trailing edge, $\zeta = \zeta_{max}$, to the outer boundary, $\zeta = \zeta_{min}$, along the vortex sheets.

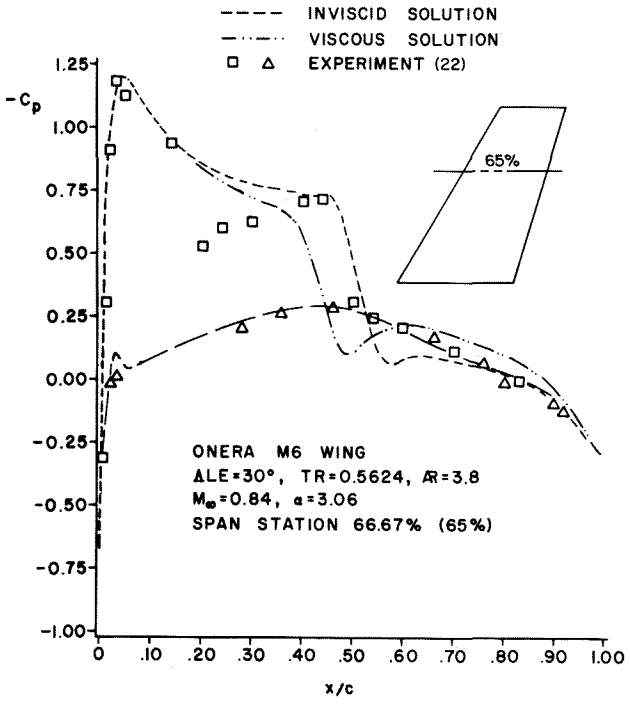

Figure 7. Pressure Coeficient, Wing M6, η = 65%

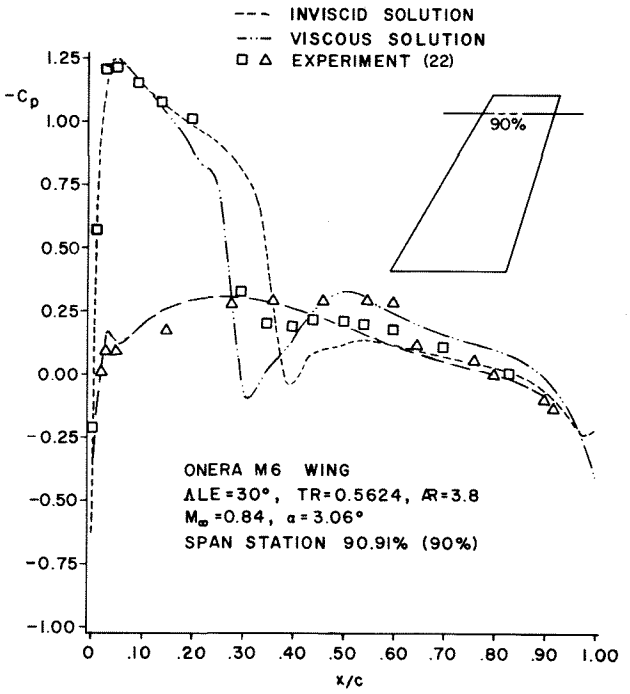

Figure 8. Pressure Coeficient, Wing M6, η = 90%

Including the small disturbance term in each contravariant velocity components as the boundary condition, the viscous effect can then be considered during the iteration process.

V. RESULTS AND DISCUSSIONS

The objective of this study is not only to improve the computational accuracy but also to maintain the computational efficiency. An AMDAHL 470 computer was used. The computations were made in two steps. The first step was to genetrate the grid which was used for both inviscid and viscous computations. The second step was to solve for the density and the velocity potential in the flowfield with the inviscid and the viscous boundary conditions. The comparison of computational time was given for the second step only.

Several wings were studied from relatively weak shock to moderately-strong shock situations:

A. Weak Shock Stiuations

The experimental data of Hinson and Burges' (19) Wing C of high-sweep ($\Lambda_{LE} = 45^{o}$) and high-taper (TR = 0.3) with a twist of 8 degrees and 2.6 aspect ratio was calculated for $M_{\infty} = 0.818$ and $\alpha = 4.952$. Figure 4 shows the a comparison between the inviscid and the viscous solutions with the experimental data of Hinson and Burges (19) and Keener (20) for the span station of 30%. The deviation between the two sets of experimental data is much more significant than the difference between the inviscid and viscous solutions. Moreover the inviscid solution took 16.66 minutes for 82 iterations while the viscous solution took 18.26 minutes for the same number of iterations. Comparisons of the inviscid solution whith experimental data at other span stations were

discussed by Holst et al. (21). For weak shock situations, the inviscid solution gives accurate results, viscous correction is not necessary.

B. Moderately-Strong Shock Situations

1. ONERA M6 Wing

The experimental data of Schmitt and Charpin (22) for the ONERA M6 Wing with leading edge sweep of 30^{o}, taper ratio of 0.56 and aspect ratio of 3.8 was computed for $M_{\infty} = 0.84$ and $\alpha = 3.06$. Figures 5, 6, 7, and 8 show the results of the inviscid and visous solutions in comparison with the experimental data at span stations of 20%, 44%, 65%, and 90%, respectively. Interacting with the boundary layer, the shock waves moved toward the leading edge by approximately 6% of the chord length at the span stations closer to the fuselage as shown in Figures 5 and 6; while the shock waves moved toward the leading edge by about 10% of the chord length at the span stations closer to the wing tip as shown in Figures 7 and 8. The viscous solution gave better agreement with the experimental data for both shock positions and pressure distributions. The viscous solution took 58 iterations with 23.73 minutes of computer time while the inviscid solution took 52 iterations with 20.93 minutes of computer time. The increase in computational time was about 13%.

2. Wing A

The experimental data of Hinson and Burges (19) for Wing A with leading edge sweep of 27^{o}, taper ratio of 0.4, aspect ratio of 8.0 and 4.8^{o} twist between root and tip was computed for $M_{\infty} = 0.80$ and $\alpha = 1.60$. Figures 9, 10, 11, 12, and 13 show the results of the inviscid and viscous solutions in comparison with the experimental data at $M_{\infty} = 0.80$ and $\alpha = 2.94$ for span stations 15%, 30%, 50%, 70%, and 95%, respectively. A moderately-strong shock wave as well as a significant after loading occured at every span station. Again the viscous solution gave better agreement with the experimental data for both shock positions and pressure distributions. It took 93 iterations with 20.93 minutes to converge to the viscous solution and 99 iterations with 20.29 minutes to converge to the inviscid

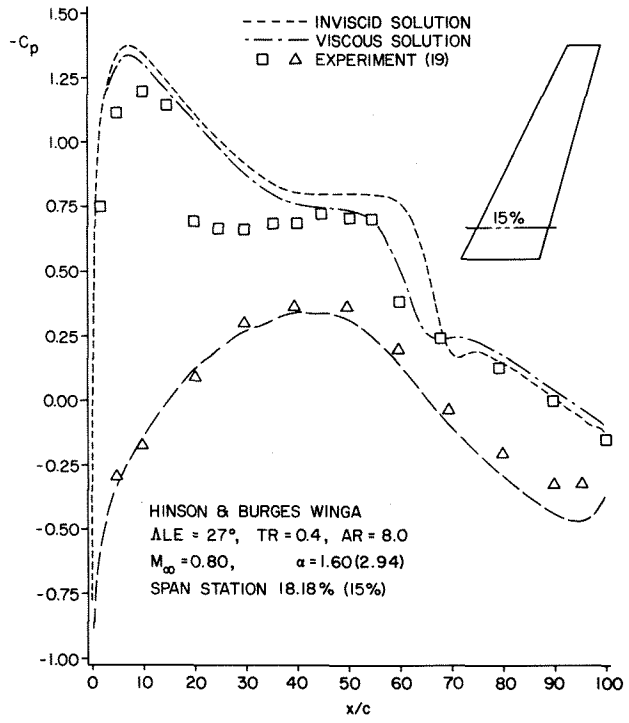

Figure 9. Pressure Coeficient, Wing A, η = 15%

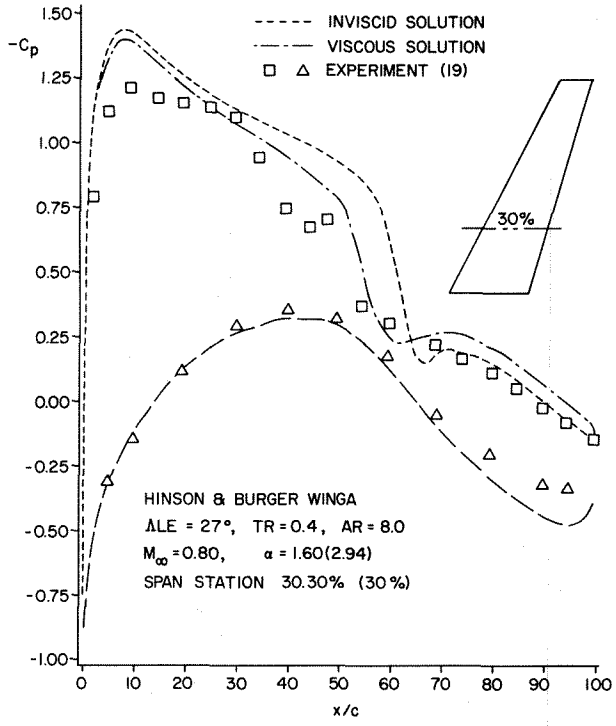

Figure 10. Pressure Coefieient, Wing A,η = 30%

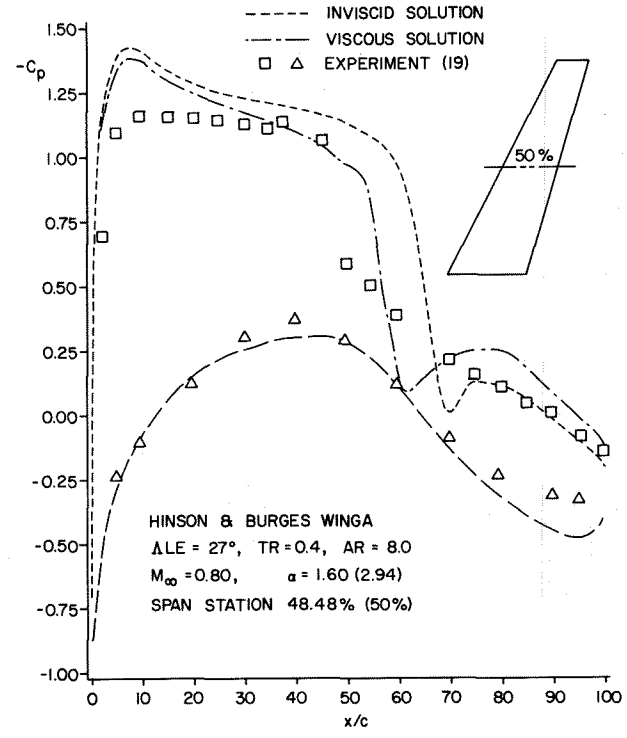

Figure 11. Pressure Coeficient, Wing A,η = 50%

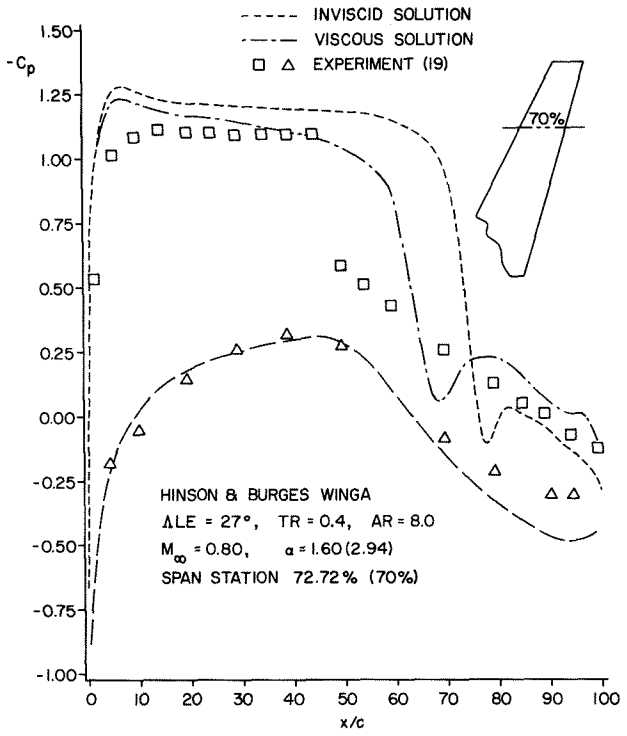

Figure 12. Pressure Coeficient, Wing A, η = 70%

solution. Consideration of the viscous effect reduced the number of supersonic points in the flowfield, thus reduced the number of iterations for the converged solution. The net increase in computational time was 3%.

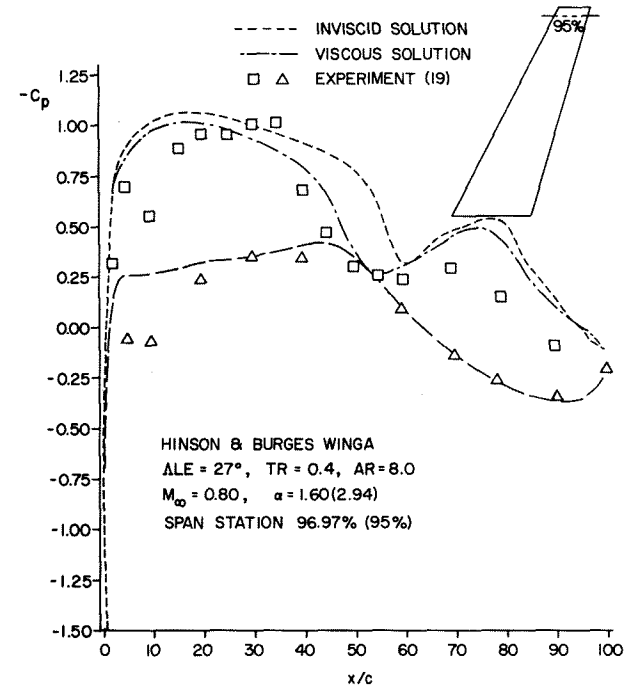

Figure 13. Pressure Coeficient, Wing A, η = 95%

VI. CONCLUSIONS

Full-potential solution is the most economical method for transonic wing analysis. TWING is yet the most efficient code for this purpose. Depending upon the shock strength, the following conclusions are reached:

1. For Weak Shock Situations:

   Solutions of TWING, which imposed the Kutta condition at the trailing edge, gave good correlation with experimental data at a reasonable amount of computer time. Viscous correction is not necessary.

2. For Moderately-Strong Shock Situations:

   Viscous correction is needed to improve the shock position and the pressure distribution. However, the increase in computer time does not have to be substantial. The present study indicated that a 13.5% and a 3% increases in computer time were needed for the ONERA M6 Wing and the Wing A, respectively.

REFERENCES

1. Pulliam, T. H. and Steger, J. L., "Implicit Finite-Difference Simulations of Three-Dimensional Compressible Flow", AIAA Journal, Vol. 18, 1980, pp. 159-167.

2. Steger, J. L., "Implicit Finite-Difference Simulation of Flow About Arbitrary Geometries with Application to Airfoils", AIAA Paper 77-665, Albuquerque, New Mexico, June 27-29, 1977.

3. Ballhaus, W. F. and Goorjian, P. M., "Implicit Finite-Difference Computation of Unsteady Transonic Flows About Airfoils", AIAA Journal, Vol. 15, No. 12, 1977, pp. 1728-1735.

4. Holst, T.L., "A Fast, Conservative Algorithm for Solving the Transonic Full-Potential Equation", Proc. AIAA 4th Computational Fluid Dynamics conference, Williamsburg Virginia, July 23-24, 1979, pp. 109-121.

5. Yoshihara, H. and Zonars, D., "An Analysis of Pressure Distributions on Planar Supercritical Profiles With and Without Jet Flaps At High Reynolds Numbers", GDCA-ERR-1964, December 1971.

6. Nash, J. and Scruggs, R., "An Automated Procedure For Computing the Three-Dimensional Transonic Flow over Wing Body Combinations, Including Viscous Effect", AFFDL-TR77-122, Vol. III, Grumman Aerospace Corporation, October 1977.

7. Melnik, R. E., Chow, R. R., Mead, H. R. and Jameson, A., "An Improved Viscid/Inviscid Interaction Procedure for Transonic Flow over Airfoils", NASI-12426, Grumman Aerospace Corporation, February 1980.

8. Green, J. E., Weeks, D. J., and Brooman, J. N. F., "Prediction of Turbulent Boundary

Layers and Wakes in Compressible Flow by a Lag-Entrainment Method", Report Memoranda 3791, Royal Aeronautical Establishment, England, 1977.

9. Sasman, P. K. and Cresci, R. J., "Compressible Turbulent Boundary Layer with Pressure Gradient and Heat Transfer Transfer", AIAA Journal, Vol. 4, No. 1 1966, pp. 19-25.

10. Mager, A., "Transformation of the Compressible Turbulent Boundary Layer", Journal of Aerospace Science, Vol. 25, No. 5, 1958, pp. 305-311.

11. Tetervin, N., "The Application of the Reference-Enthalpy Method to Friction Formulas", Journal of Aerospace Science, Vol. 29, 1962, p. 493.

12. McNally, W. D. , "FORTRAN Program for Calculating Compressible Laminar and Turbulent Boundary Layers in Arbitrary Pressure Gradients", NASA TN D-5681, 1970.

13. Lee, S. C. and Van Dalsem, W. R., "Numerical Simulation of Steady Transonic Flow about Airfoils", Proc. AIAA Computational Fluid Dynamics Conference, Palo Alto, CA., June 22-23, 1981.

14. Lee, S. C., "A Fast Viscous Correction Method for Unsteady Transonic Flow about Airfoils", AIAA Paper 83-0264, Jan. 1983.

15. Holst, T. L. and Thomas, S. D., "Numerical Solution of Transonic Wing Flow Fields", AIAA Paper 82-0105, Jan. 1982.

16. Caughey, D. A. and Jameson, A., "Numerical Calculation of Transonic Potential Flow about Wing-Body Combinations", AIAA Journal, Vol. 17, No. 2, 1979, pp. 175-181.

17. Cohen, C. B. and Roshotko, E., "The Compressible Boundary Layer with Heat Transfer and Arbitrary Pressure Gradient", NACA TR-1294, 1956.

18. Lighthill, M. J., "On Displacement Thickness", J. Fluid Mech., Vol. 4, 1958.

19. Hinson, B. L. and Burdges, K. P., "Acquisition and Application of Transonic Wing and Far-Field Test Data for Three-Dimensional Computational Method Evaluation", AFSOR-RT-80-0421, March 1980.

20. Keener, E., Ames Research Center, Private Communication, 1982.

21. Holst, T. L., Subramanian, N. R. and Thomas, S. D., "The Efficient Solution of Transonic Wing Flow Field", The 2nd Symposium on Numerical and Physical Aspects of Aerodynamic Flows, Long Beach, CA. 1983.

22. Schmitt, V. and Charpin, F., "Pressure Distributions on the ONERA-M6-Wing at Transonic Mach Numbers," AGARD Report AR-138, May 1979.